Vol. 39 (2008) ACTA PHYSICA POLONICA B No 3

COMPARISON BETWEEN ZERO-RANGE AND FINITE-RANGE CALCULATIONS OF TOTAL REACTION CROSS-SECTIONS FOR HALO NUCLEI

S.S. Al-Thoyaib

Physics Department, College of Science, Qassim University
Al-Qassim, Oyoun Al-Jawa, PO Box 151, Kingdom of Saudi Arabia
salthoyaib@yahoo.com

(Received July 5, 2007; revised version received November 27, 2007)

Total cross-sections of the halo nuclei in both the zero- and the finite-ranges are calculated at energy range of 25–800 MeV$/n$, by using the carbon nuclei as a probe. The calculations are based on the Optical Limit Approximation (OLA) of the Glauber theory and are done for Li, Be and B isotopes using the finite and the zero range interactions. We found that the total cross-sections depend slightly on the nuclear density. On the other hand, there is a discrepancy between the calculated results of both ranges in the surface region of the reaction probability. The theoretical results for the zero- and the finite-range are compared with experimental data. We found that the zero-range predictions are consistent with experimental data more than the finite-range.

PACS numbers: 24.10.–i, 24.10.Ht, 25.60.Dz, 21.45.+v

1. Introduction

Nuclear physicists discovered twenty years ago that some of the lightest nuclei can have a matter radius as large as those found in the heaviest naturally occurring elements [1]. This was explained by weakly bound nucleons that form a dilute cloud around a central nuclear core [2]. Such a structure is called a neutron halo.

These extended nuclei behave very differently from ordinary ones. Normal nuclei are difficult to excite or break apart, but halo nuclei are fragile objects. They are larger than normal nuclei and interact with them more easily as well. In fact, the halo is a quantum phenomenon that does not obey the laws of classical physics. A schematic picture for the structure of the two-neutron halo nucleus ^{11}Li compared to the nucleus of lead-208, which has almost 20 times more nuclear particles, is shown in Fig. 1.

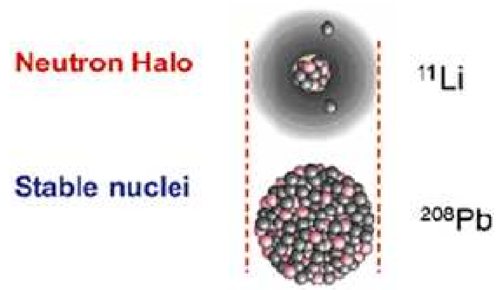

Fig. 1. Comparison between the halo nucleus ^{11}Li and the stable nucleus ^{208}Pb.

The study of nuclei far from the valley of stability is an emerging frontier field in nuclear physics. The study of exotic nuclei provides new and exciting opportunities for probing the details of the nuclear force and understanding exactly how nuclei are put together and how they react. Furthermore, the properties of exotic nuclei are key for understanding the production of the elements. Additionally, the study of exotic nuclei is essential in many fields of astrophysics, where they are used to model stars, supernova, X-flares and all the cosmic cauldrons where the elements were created.

Up to now much effort has been made to the study of neutron halo structure, such as the discovery of neutron halo nuclei ^{6,8}He, ^{11}Li, ^{11,14}Be [3] and the recent work on ^{19}C [4,5]. At the same time, some work has been performed on proton halo nuclei, *e.g.* ^{8}B and ^{17}Ne. Due to Coulomb effect, the formation of proton halo is more difficult and complicated compared to neutron halo structure.

Experimental study of unstable nuclei has considerably advanced via the technique of using secondary radioactive beams. The quantities measured in the study include various inclusive cross-sections, for example, reaction or interaction cross-sections, nucleon-removal cross-sections, Coulomb breakup cross-sections and momentum distributions of a fragment.

These quantities have played a pivotal role in revealing the nuclear structure of unstable nuclei, particularly halo structure near the drip line [6]. The total reaction cross-section (σ_{R}) is one of the most fundamental quantities characterizing the nuclear reactions as well as for probing for nuclear structure details.

Several methods are available to study the total reaction cross section, such as the multi-step scattering theory of Glauber [7], the transport model method of Ma *et al.* [8] and the semi-empirical formula of Kox *et al.* [9] and Shen *et al.*, [10] *etc.* For the first one, because of its simplicity, the optical limit approximation (OLA) of the Glauber approach is the most common used method [7]. The optical phase in the OLA is given by a functional of the densities of the projectile and the target.

The aim of this work is to calculate the total reaction cross-sections in the zero-range and finite-range for ^{12}C, $^{8-17}$B, $^{7-14}$Be and $^{6-9,11}$Li isotopes incident on a ^{12}C target in the energy range of 25–800 MeV$/n$. It should be noted that this work is motivated by the comments of the referee of our previous paper [11].

The out line of this paper is as follows: in Section 2 we briefly discuss the formalism used in our calculations. Section 3 shows the results. Finally we present the summary in Section 4.

2. Eikonal approximation of the Glauber theory

Within the Eikonal approximation, the trajectory of the projectile is approximated by a straight line, while the Adiabatic approximation neglects the excitation energies of the colliding nuclei. These approximations are needed to derive a simple, tractable expression for the scattering amplitude. Under these approximations the scattering amplitude is given by

$$f_{\alpha\beta}(\theta,\phi) = \frac{iK}{2\pi}\int db\, e^{-iq.b}\left\langle \Psi_\alpha^{(\mathrm{P})}\Psi_\beta^{(\mathrm{T})}\middle| 1-e^{i}\sum_{i\epsilon P}\sum_{j\epsilon T}\chi_{NN}{}^{b+s_i^{(\mathrm{P})}-s_j^{(\mathrm{T})}}\middle|\Psi_0^{(\mathrm{P})}\Psi_0^{(\mathrm{T})}\right\rangle , \tag{1}$$

where q is the momentum transferred from the target to the projectile, b a two-dimensional impact-parameter vector perpendicular to the z-direction and $s_i^{(\mathrm{P})}$ is the projection onto the x–y-plane of the nucleon position vector relative to the projectile's c.m., $r_i^{(\mathrm{P})} - R_{\mathrm{c.m.}}^{(P)}$.

The wave function $\Psi_\alpha^{(P)}$ denotes the projectile's intrinsic state specified by a quantum number α with its c.m. part being dropped ($\alpha = 0$ stands for the ground state). Similarly, the target state is denoted by $\Psi_\beta^{(\mathrm{T})}$. Thus, f_{00} stands for the elastic scattering amplitude. See, for example, Refs. [7,12] for more details.

The phase-shift function χ_{NN} in Eq. (1) is a basic ingredient for the scattering amplitude. It describes the NN scattering and is related to the NN potential V_{NN} by

$$\chi_{NN}(b) = -\frac{1}{\eta\vartheta}\int_{-\infty}^{+\infty} dz\, V_{NN}(b+z\hat{z})\,, \tag{2}$$

where ϑ is the asymptotic velocity of the relative motion between the projectile and the target and $\hat{z}$ is a unit vector in the z-direction. The NN potential contains complicated spin–isospin dependence, so χ_{NN} in general becomes an operator acting in that space. The use of such an operator in Eq. (1) is extremely involved, and here it is treated as just a function by ignoring the spin–isospin dependence as is usually done. The NN profile function $\Gamma_{NN}(b)$ is introduced and often parameterized in the form [13]

$$\Gamma_{NN}(b) = 1 - e^{i\chi_{NN}(b)} = \frac{1-i\alpha}{2\pi}\,\omega\sigma_{NN}e^{-\omega b^2}\,, \tag{3a}$$

$$\Gamma_{NN}(b) = \frac{1-i\alpha}{4\pi\beta}\,\sigma_{NN}e^{-b^2/2\beta} \qquad (\mathrm{finite}-\mathrm{range})\,, \tag{3b}$$

$$\Gamma_{NN}(b) = \frac{1-i\alpha}{2}\,\sigma_{NN}\delta(b) \qquad (\mathrm{zero}-\mathrm{range})\,. \tag{3c}$$

Here σ_{NN} is the total NN cross section and the parameters α and ω are determined so as to fit the NN elastic differential cross section as well as the NN reaction cross section at relevant energy.

To get the elastic scattering amplitude f_{00} we need to calculate the phase-shift function $\chi(b)$

$$e^{i\chi(b)} = \left\langle \Psi_0^{(\mathrm{P})}\Psi_0^{(\mathrm{T})}\middle| \prod_{i\epsilon P}\prod_{j\epsilon T}\left[1-\Gamma_{NN}(b+s_i^{(\mathrm{P})}-s_j^{(\mathrm{T})}\right]\middle|\Psi_0^{(\mathrm{P})}\Psi_0^{(\mathrm{T})}\right\rangle\,. \tag{4}$$

The above matrix element contains a multi-dimensional integration, which is obviously not easy to perform in general. Recently, it has been demonstrated [14] that the phase-shift function can be evaluated by Monte Carlo method without approximation. However, for simplicity the optical limit approximation is routinely used. In the following, we explain the optical limit approximation.

2.1. The optical limit approximation

The optical limit approximation makes it possible to calculate the optical phase through the densities of the projectile and the target as follows

$$e^{i\chi_{\mathrm{OLA}}(b)} = \exp\left\{-\iint dr\,ds\,\rho_{_P}(r_1)\rho_{_T}(r_2)\Gamma_{NN}(b+s_1-s_2)\right\}\,, \tag{5}$$

where $s_1(s_2)$ is the projection of $r_1(r_2)$ in x–y plane, $\rho_{_P}(r_1)$ and $\rho_{_T}(r_2)$ are the densities of the projectile and target, respectively.

The needed input to the above equation are the densities of the projectile and the target and the values of the NN-parameters. The densities which we used here were taken from [15], while the values of the parameters were taken from [16].

For the finite-range, we use Eq. (3b) for the expression of the NN profile function, while we use Eq. (3c) for the zero-range.

2.2. Reaction cross section in the Eikonal approximation

The Eikonal model provides a convenient framework for calculating integrated cross-sections for a variety of processes involving peripheral collisions between composite projectiles and stable targets. The reaction cross section for a projectile-target collision is calculated by integrating the reaction probability with respect to the impact parameter b

$$\sigma_{\mathrm{R}} = \int db \left(1 - \left|e^{i\chi(b)}\right|^2\right) , \tag{6}$$

where the phase shift function χ is obtained from Eq. (5). Here, we define the reaction probability as

$$P(b) = 1 - \left|e^{i\chi(b)}\right|^2 . \tag{7}$$

3. Results and discussion

The total reaction cross-sections for $^{12}\mathrm{C} + {}^{12}\mathrm{C}$ at different energies from 25 to 800 MeV/n are calculated. Results for both the finite-range and the zero-range are presented. In Fig. 2, we compared the finite-range and the zero-range calculations with the experimental data from Ref. [9].

As can be seen from the figure there is a good agreement between the experimental data and the zero-range calculations, conversely the finite-range overestimates the experimental data in the region of 100–300 MeV/n.

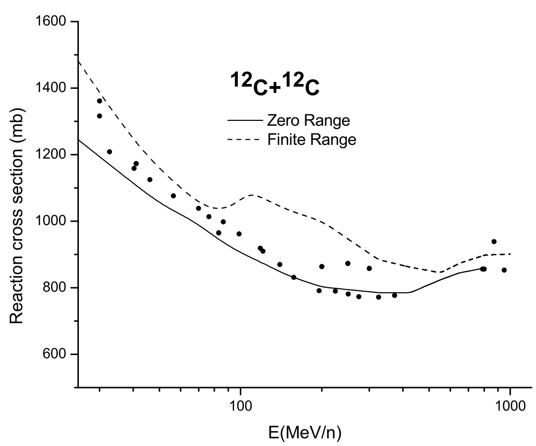

Fig. 2. Comparison between the reaction cross-sections calculated for $^{12}\mathrm{C} + {}^{12}\mathrm{C}$ at different energies with the finite-range (dashed line) and zero-range (solid line). The experimental data are taken from [9].

In Fig. 3, the total reaction cross-sections for ^{14}Be incident on a ^{12}C target (left panel) and for ^{11}Be incident on a ^{12}C target (right panel), in case of the finite-range and the zero-range calculations are compared.

Both ^{11}Be and ^{14}Be are halo nuclei, from the calculations the difference between the zero-range and the finite-range at 25 MeV/n are 234 mb and 241 mb while at 800 MeV/n are 37 mb and 39 mb, respectively. By comparing these values with those of ^{12}C + ^{12}C which are 236 mb at 25 MeV/n and 39 mb at 800 MeV/n, we found that the difference between the finite-range and the zero-range did not depend on the system. Rather it depends only on the energy. The finite range overestimated the zero range by 16% and 5% at 25 MeV/n and 800 MeV/n, respectively.

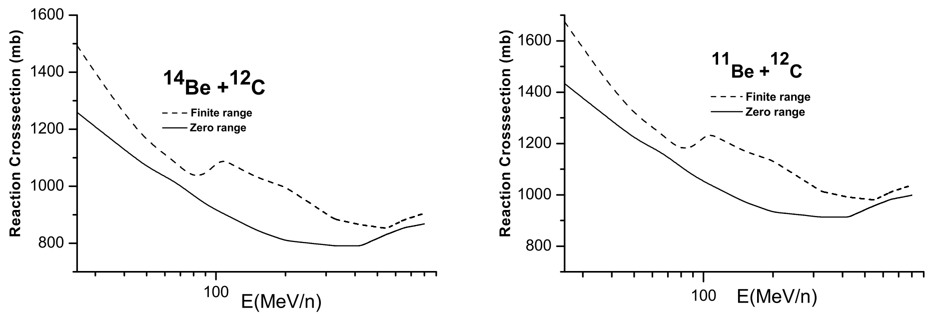

Fig. 3. Comparison between the reaction cross-sections calculated for ^{11}Be + ^{12}C (right panel) and ^{14}Be + ^{12}C (left panel) at different energies with the finite-range (solid line) and the zero-range (dashed line).

In Fig. 4 we compared the total reaction cross-sections for $^{7-14}$Be incident on a ^{12}C target in the case of finite-range and zero-range calculations at fixed energy 25 MeV/n (left panel) and at 800 MeV/n (right panel). In both cases, there was a difference about to be fixed.

The reaction cross-sections in case of the finite-range exceeded that in the case of zero-range, this result supports what we found in Fig. 3. As shown in Figs. 2, 3 and 4, the results with finite-range interaction are systematically larger than those of zero-range one. This behavior could be understood as follows: The factor β of finite-range in Eq. (5) increased the surface part of the density and since the reaction cross section depends mostly on the surface, so the reaction cross section increased.

To see this effect, we plot in Fig. 5 the reaction probability for ^{12}C + ^{12}C for both zero-range and finite-range cases. Thus, it seems reasonable to argue that the reaction probability with finite-range increases in the surface and that comes in-line with the course of our discussion.

Moreover, it is interesting to see in what region of the reaction probability the difference between ^{12}Be and ^{14}Be occurs, since the structure of ^{14}Be is $^{12}\mathrm{Be} + n + n$.

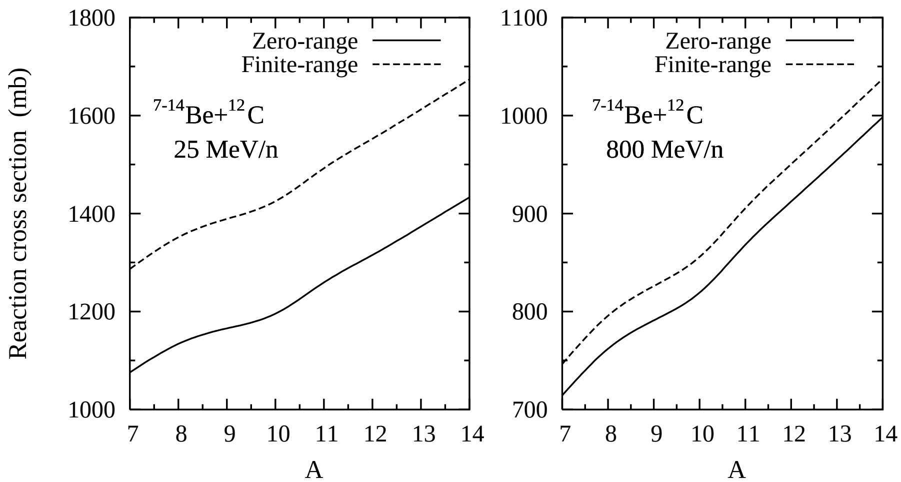

Fig. 4. The reaction cross-sections for $^{7-14}$Be $+^{12}$C calculated at $25\,\mathrm{MeV}/n$ (left panel) and at $800\,\mathrm{MeV}/n$ (right panel). Dashed line is for the zero-range while solid line is for the finite-range calculation.

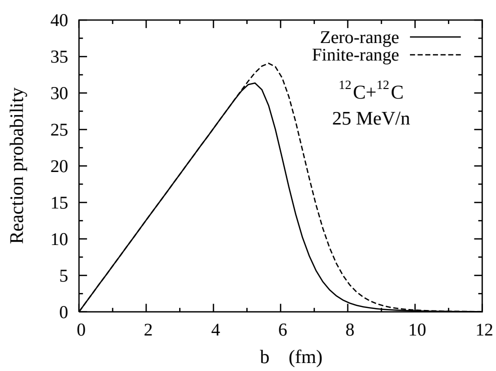

Fig. 5. The reaction probability for ^{12}C + ^{12}C in case of the finite-range and the zero-range calculated at energy of $25\,\mathrm{MeV}/n$.

In Fig. 6, we plot the reaction probability of both ^{12}Be and ^{14}Be as a function of the impact parameter at $25\,\mathrm{MeV}/n$. As one can see, the difference appears in the surface region. This is simply because the difference between ^{12}Be and ^{14}Be is a two neutron in the surface.

The effect of the density on the reaction cross section is discussed in Fig. 7, where we compare the reaction probability in the case of two densities "Relativistic Mean Field (RMF) and the Extension of this formalism with field theory motivated effective Lagrangian approach (E-RMF)" mentioned in Ref. [15]. The upper graph compares the reaction probability for ^{14}Be + ^{12}C reaction at energy of $25\,\mathrm{MeV}/n$ for the two densities.

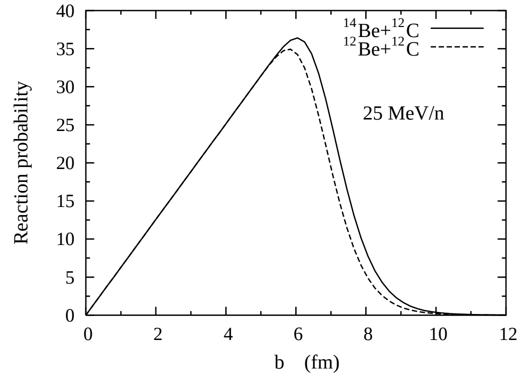

Fig. 6. Comparison between the reaction probability for ^{14}Be and its core at energy of $25\,\mathrm{MeV}/n$.

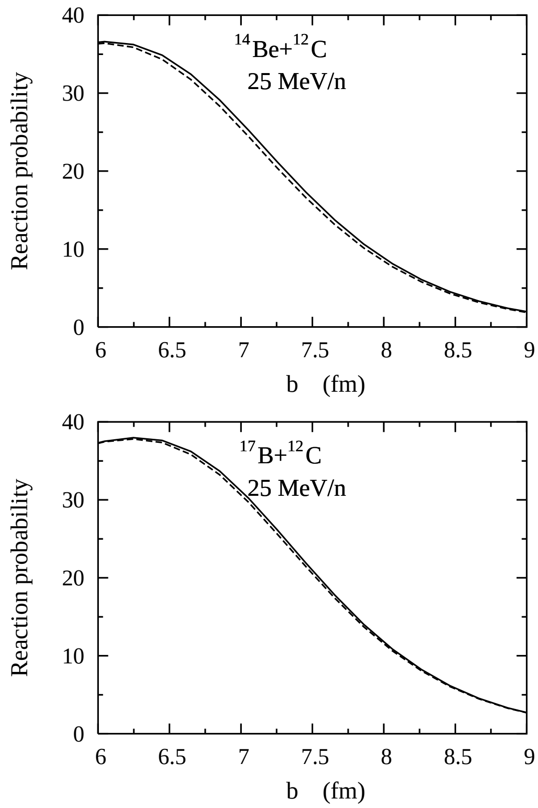

Fig. 7. The reaction probability of the two densities in Ref. [15] (RMF (solid), E-RMF (dashed)) at energy of $25\,\mathrm{MeV}/n$, for $^{14}\mathrm{Be} + {}^{12}\mathrm{C}$ (upper graph) and for $^{17}\mathrm{B} + {}^{12}\mathrm{C}$ (lower graph).

The lower graph compares the reaction probability for ^{17}B + ^{12}C reaction at energy of 25 MeV/n for the two densities. We have chosen this energy to maximize the difference between the reaction probability for both systems. As we see, there is almost no difference between the two densities. This is why we have used only one density in our calculations.

Fig. 8 compares the finite-range and the zero-range calculations with the experimental values (when available) for $^{8-17}$B, $^{7-14}$Be and $^{6-9,11}$Li isotopes incident on a ^{12}C target.

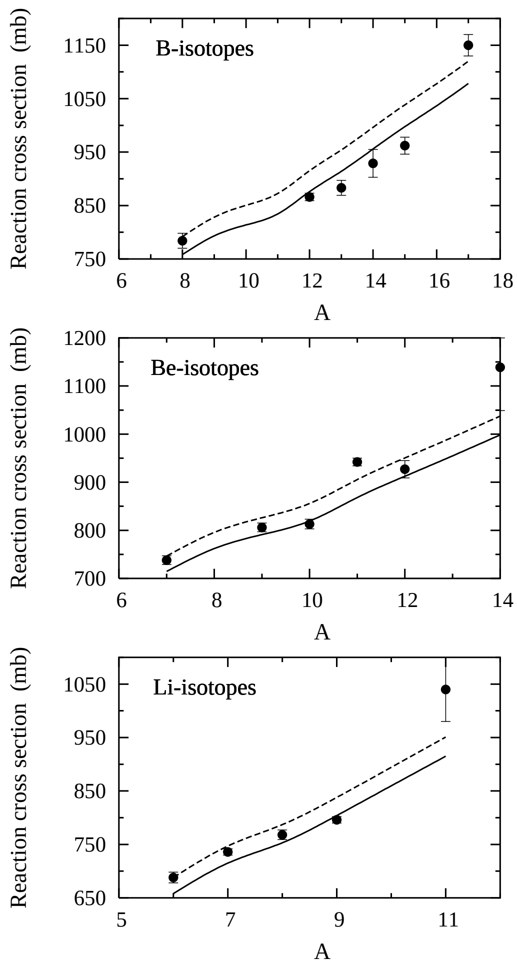

Fig. 8. The reaction cross-sections for Li, B and Be isotopes incident on a ^{12}C target at energy of 800 MeV/n in comparison with the experimental data. The solid line shows the calculations with the zero-range and the dashed line represents the calculations with the finite-range. The experimental data are taken from Ref. [16].

In the first graph, the finite-range calculations are greater than the zero-range ones by about 39 mb. The experimental values agree with the finite-range calculations for ^{8}B and more than the zero-range calculations by 26 mb, while for ^{12}B the experimental values agree with the zero-range calculations but they exceed the finite-range calculations by 48 mb.

For $^{13-15}$B, the experimental values are less than the zero-range calculations by 31, 27 and 36 mb, respectively, while they are less than the finite-range calculations by 71, 67 and 76 mb, respectively. However, for ^{17}B they are greater than the finite-range calculations by 30 mb and greater than the zero-range calculations by 72 mb. The second graph shows an increment in the finite-range calculations by about 37 mb than the zero-range calculations.

The experimental values harmonize well with both calculations for ^{7,9,12}Be. While for ^{10}Be the experimental values are consistent with the zero-range calculations, but are less than the finite-range calculations by 43 mb. Concerning ^{11}Be, the experimental values are greater than the finite-range calculations by 38 mb and exceed the zero-range calculations by 75 mb. For the last isotope ^{14}Be, the experimental values exceed the finite-range calculations by 102 mb and exceed the zero-range calculations by 142 mb. In the third graph, the finite-range calculations outstrip the zero-range calculations by about 33 mb. The experimental values are in good agreement with both the finite-range and the zero-range calculations for ^{7,8}Li and agree with the finite-range calculations for ^{6}Li, but overstep the zero-range calculations by 32 mb. As for ^{9}Li the experimental values go in-tandem with the zero-range calculations but they are less than the finite-range calculations by 41 mb.

The experimental values for ^{11}Li go beyond the finite-range calculations by 90 mb which overtake the zero-range calculations by 36 mb.

4. Summary

We have calculated the reaction cross-sections of some light exotic nuclei using the optical limit approximation of Glauber. We have used both finite-range and zero-range interactions. We found that zero-range interaction gives good fitting to the experimental data better than finite-range. As we go from high energy to low energy there is a sudden decrease in the reaction cross-sections. The zero-range calculations explain that this behavior is due to the finite range parameter beta, which is not well determined. These calculations support our previous finding in Ref. [11]. In addition, we found that the difference between the zero-range and the finite-range is in the surface region of the reaction probability. The reaction cross-sections depend little on the nuclear density. Finally, we found a good agreement between our calculations and the experimental data at high energies.

REFERENCES

[1] I. Tanihata, H. Hamagaki, O. Hashimoto, Y. Shida, N. Yoshikawa, K. Sugimoto, O. Yamakawa, T. Kobayashi, N. Takahashi, *Phys. Rev. Lett.* **55**, 2676 (1985).

[2] P.G. Hansen, B. Jonson, *Europhys. Lett.* **4**, 409 (1987).

[3] I. Tanihata *et al., Phys. Lett.* **B160**, 380 (1985); I. Tanihata *et al., Phys. Lett.* **B287**, 307 (1992).

[4] D. Bazin *et al., Phys. Rev. Lett.* **74**, 3569 (1995); D. Bazin *et al., Phys. Rev.* **C57**, 2156 (1998).

[5] A. Ozawa *et al., Eur. Phys. J.* **A13**, 163 (2002).

[6] I. Tanihata, *J. Phys. G* **22**, 157 (1996).

[7] R.J. Glauber, *Lectures in Theoretical Physics*, Interscience, New York 1959, Vol. 1, p. 315.

[8] Y.G. Ma *et al., Phys. Lett.* **B302**, 386 (1993); Y.G. Ma *et al., Phys. Rev.* **C48**, 850 (1993).

[9] S. Kox *et al., Phys. Rev.* **C35**, 1678 (1987).

[10] W.Q. Shen *et al., Nucl. Phys.* **A491**, 130 (1989).

[11] S.S. Al-Thoyaib, *Journal of King Saud University*, in press.

[12] See, for example, Y. Suzuki, R.G. Lovas, K. Yabana, K. Varga, *Structure and Reactions of Light Exotic Nuclei*, Taylor & Francis, London 2003.

[13] B. Abu-Ibrahim, Y. Ogawa, Y. Suzuki, I. Tanihata, *Comput. Phys. Commun.* **151**, 369 (2003).

[14] K. Varga, S.C. Pieper, Y. Suzuki, R.B. Wiringa, *Phys. Rev.* **C66**, 034611 (2002).

[15] A. Shukla *et al.*, `nucl-th/0703070 v1`.

[16] A. Ozawa, T. Suzuki, I. Tanihata, *Nucl. Phys.* **A693**, 32 (2001).